ChemComm

COMMUNICATION

View Article Online
View Journal | View Issue

Cite this: *Chem. Commun.*, 2017, 53, 8474

Received 12th May 2017,
Accepted 6th July 2017

DOI: 10.1039/c7cc03709k

rsc.li/chemcomm

Contorted polycyclic aromatic hydrocarbons with cove regions and zig-zag edges†

Yulan Chen, [ab] Tomasz Marszalek,[a] Torsten Fritz, [c] Martin Baumgarten, [a] Manfred Wagner,[a] Wojciech Pisula,[ad] Long Chen *[ab] and Klaus Müllen*[a]

A series of tetrapyrene-fused benzocoronenes was synthesized by a "bottom-up" approach, which offers a facile access to extended polycyclic aromatic hydrocarbons with concave π-surfaces, cove regions and zig-zag edges.

Graphene nanostructures with zig-zag edges have attracted great interest, since they can not only lead to nonbonding π-electron states in the zig-zag edge regions, but also crucially influence molecular characteristics like electronic properties, reactivity, stability, three-dimensional shape and solubility.[1–4] As a class of finite graphene cutouts (*i.e.*, nanographenes), disc-shaped contorted polycyclic aromatic hydrocarbons (PAHs) hold great promise for potential (opto-)electronic applications, whose functionality deviates based on their high degree of extended conjugation, concave π-surfaces and tunable edge peripheries.[5–8] To date, however, only a limited number of structurally defined zig-zag shaped nanographene molecules have been reported.[8b]

Besides nanofabrication techniques,[9,10] bottom-up organic synthesis enables precise control over the π-extension and zig-zag edge geometry of nanographene molecules and therefore could be an efficient approach to modulate their optical and electronic properties. In the past decade, contorted PAH chemistry has seen remarkable progress (Scheme 1).[11–19] For example, as shown in Scheme 1, Nuckolls and coworkers reported the facile synthesis of contorted hexabenzocoronene (c-HBC) and contorted octabenzocircumbiphenyl (c-OBCBs).[8b] Of particular interest was the recent attachment of thiophene segments to the anthradithiophene-5,11-dione skeleton followed by oxidative cyclodehydrogenation to prepare contorted thiophene-annulated coronenes (HTCs: coroneno[1,2-*b*:4,3-*b*′:5,6-*b*″:7,8-*b*‴:10,9-*b*⁗,11,12-*b*⁗′]hexathiophene).[16] Motivated by the synthesis of extended coronenes with defined edges, we herein reason that, rather than thiophene units, the fusion of pyrene moieties would result in larger coronenes with zig-zag edges and cove regions, since the shape of pyrene provides the possibility for the build-up of differently rimmed PAHs. It is well accepted that the rim structure of PAHs crucially influences the molecular characteristics like electronic properties, reactivity, stability, three-dimensional shape and solubility.[5] To this end, we envisaged a series of tetrapyrene-fused coronenes (**TPC**, Scheme 1) and established a straightforward route to such large π-conjugated aromatic discs. The structures and physical properties of **TPC**s were unambiguously elucidated by a broad combination of spectroscopic analyses and theoretical studies.

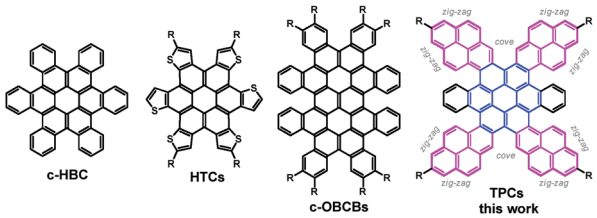

Scheme 1 Representative examples of disc-shaped contorted PAHs.

The synthetic strategy towards the targeted **TPC**s is based on the (1) regio-controlled functionalization on 2- and 2,7-pyrenes,[20] and (2) solution-mediated cyclodehydrogenation (Scholl reaction) of **3** to produce π-extended pyrene–coronene conjugates.[21] The structures and synthesis of the target molecules **TPCa–c** are presented in Scheme 2. The key building block 1,1,8,8-tetrabromobisolefin **1** was prepared in a yield of 90% starting from 6,13-pentacenequinone *via* the Corey–Fuchs (CF) reaction with slight modifications.[14,16] On the other hand, the regiospecific direct C–H borylation of pyrene or 2-*tert*-butyl pyrene with an iridium-based catalyst gave 4,4,5,5-tetramethyl-2-(pyren-2-yl)-1,3,2-dioxaborolane **2a**

[a] *Max Planck Institute for Polymer Research, Ackermannweg 10, 55128 Mainz, Germany. E-mail: muellen@mpip-mainz.mpg.de*
[b] *Department of Chemistry, Tianjin University, 300072 Tianjin, P. R. China. E-mail: long.chen@tju.edu.cn*
[c] *Friedrich Schiller University Jena, Institute of Solid State Physics, Helmholtzweg 5, 07743 Jena, Germany*
[d] *Department of Molecular Physics, Lodz University of Technology, Zeromskiego 116, 90-924 Lodz, Poland*

† Electronic supplementary information (ESI) available. CCDC 1517012 and 1517013. For ESI and crystallographic data in CIF or other electronic format see DOI: 10.1039/c7cc03709k

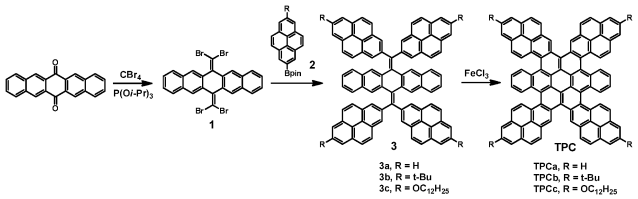

Scheme 2 Synthetic route to **TPC**s.

or 2-(7-(*tert*-butyl)pyren-2-yl)-4,4,5,5-tetramethyl-1,3,2-dioxaborolane **2b**, respectively, according to a recently established procedure.[20] In the case of dodecyloxyl substituted pyrene boronic ester **2c**, 4,4,5,5-tetramethyl-2-(pyren-2-yl)-1,3,2-dioxaborolane (**2a**) was first oxidized to 2-hydroxypyrene by H_2O_2 in 86% yield. The dodecyloxy chains were then introduced under basic conditions using K_2CO_3/butanone (yield: 87%) followed by C–H borylation at the 7-position of the pyrene, leading to **2c** in 33% yield (see the ESI†). These pyrene based boronic pinacolate esters **2a–c** can be readily incorporated into the pentacene skeleton by four-fold Suzuki–Miyaura cross-coupling with **1**, affording bis-olefin **3** in high isolated yields (80–93%). *tert*-Butyl or dodecyloxy groups were attached to the peripheries of the pyrene units to ensure solubility. These tetra-pyrenyl-dihydromethylenyl-pentacenes (**3a–c**) were fully characterized by mass-spectrometry, ^{1}H and ^{13}C-NMR spectroscopy. But as just yellow compounds only absorb visible light at around 400–450 nm, the observation is in agreement with DFT calculations for the extended π-system, demonstrating that the large torsion angles of the pyrenes ($\theta > 60^\circ$) relative to the dihydropentacene led to nearly isolated chromophores (Fig. S1, ESI†).

Single crystals of **3a** and **3b** suitable for X-ray diffraction analysis could be grown from a toluene/methanol mixture upon slow evaporation. The single-crystal structures of **3a** and **3b** from X-ray diffraction are displayed in Fig. 1 and Fig. S2 (ESI†), revealing the sterically crowded skeletons of these bis-olefins. Subsequently, further cyclization of **3a–c** to the corresponding **TPCa–c** with even extended conjugation was performed *via* the Scholl reaction. The cyclodehydrogenation worked smoothly in good yields (75–84%) when ferric chloride was chosen as an oxidant.

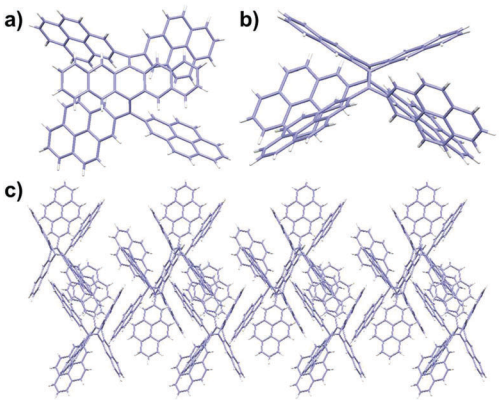

Fig. 1 Crystal structure and molecular packing of **3a** (CCDC 1517012).† (a) Top view of **3a**; (b) side view of **3a**; and (c) crystal packing of **3a** along the *a* axis.

This is surprising, since the rigid and bulky pyrene units resulted in larger steric hindrance and concomitant higher strain energy for cyclization compared to that of thiophene-fused coronenes.[14]

Arising from the non-planarity of the condensed coronene core, all target molecules could be dissolved in common organic solvents, such as methylene chloride, chloroform, and toluene. These compounds were characterized by NMR spectroscopy, mass spectrometry and elemental analysis. MALDI-TOF mass spectra of **TPCa–c** revealed single species with isotopic distributions in accordance with calculations (Fig. S3, ESI†). Thermogravimetric analysis (TGA) of **TPCa** and **TPCb** showed less than 5% weight loss up to 400 °C and a residual weight percentage of about 80–90% even at 900 °C under a nitrogen atmosphere. For **TPCc**, the dealkoxylation started already at *ca.* 230 °C (Fig. S4a, ESI†), since alkoxy substituents are far less thermostable than alkyl groups. No distinct transition was observed from 25 to 300 °C by differential scanning calorimetry (DSC) of **TPCa** and **TPCb** (Fig. S4b, ESI†).[22] In contrast, **TPCc** exhibited a distinct endothermal peak at about 44 °C of the first and second heating cycles. However, no morphology change was observed by polarized optical microscopy in the cooling and heating runs within the 25–300 °C temperature range. Therefore, the above observed endothermal peak can probably be ascribed to the reorganization of the alkoxy chains.[23,24]

The UV-vis absorption spectra of **TPCa–c** in toluene are presented in Fig. 2a, which demonstrate intense absorptions in the region ranging from 300 to 650 nm. Compounds **TPCa–c** displayed some distinct absorption bands which can be assigned to the β- and p-bands characteristic of large PAHs with rigid skeletons.[11,16] For instance, **TPCb** exhibited absorption peaks at 370 nm (pyrene subchromophores, $\varepsilon = 1.25 \times 10^5$ M^{-1} cm^{-1}) and 452 nm (β band, $\varepsilon = 1.29 \times 10^5$ M^{-1} cm^{-1}) with a shoulder at 574 nm (p band, $\varepsilon = 0.53 \times 10^5$ M^{-1} cm^{-1}) from the HOMO–LUMO transition, while the α-band is very weak and could not be separated between the β- and p-bands. These absorption features of **TPCb** are in good agreement with the calculated values (Fig. S5, ESI†). As for **TPCa** without *tert*-butyl substituents, the absorption peaks shifted hypsochromically with decreased intensity due to its significant tendency for aggregation. In contrast, the β- and p-bands of **TPCc** were distinctly red shifted to 456 and 596 nm, respectively, with decreased absorption intensity. The spin-coated films of **TPCa–c** all exhibited broad

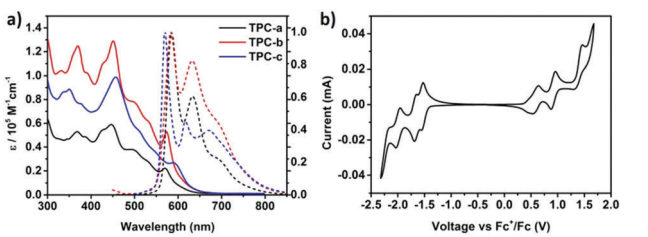

Fig. 2 (a) UV-vis spectra (solid) and photoluminescence (PL) spectra (dashed, excited at 455 nm) of **TPCa–c** (1.0×10^{-6} M in toluene); and (b) cyclic voltammetric curves of **TPCb** in DCM (0.5 mM) containing 0.1 M Bu_4NPF_6. Potentials are reported *vs.* the Fc/Fc^+ redox couple as a standard, scan rate = 50 mV s^{-1}.

absorption curves with almost no fine vibration structures (Fig. S6, ESI†), indicating a strong tendency for aggregation of **TPC**s. The three molecules displayed fluorescence emission in the orange-red region from 500 to 800 nm. Photoluminescence (PL) spectra of **TPCa** and **TPCb** showed similar shapes with the same emission peaks at *ca.* 584 nm and 634 nm, along with a spectral shoulder at 693 nm (Fig. 2a). In the case of **TPCc**, the attachment of electron-donating substituents to the four pyrenes resulted in a hypsochromic shift of 13 nm compared to that of **TPCa** and **TPCb** with an emission peak at 571 nm (Fig. 2a and Table S1, ESI†). As the largest contorted PAH synthesized so far, both absorption and emission maxima in solution for **TPCa–c** are bathochromically shifted by *ca.* 45 nm as compared to the reported c-**OBCB** (Scheme 1), reflecting the extended conjugation in **TPCa–c**.[25]

The energy levels for ionization potentials (IPs) and electron affinities (EAs) of **TPCa–c** were derived by cyclic voltammetry (Fig. 2b and Table S1, ESI†). For the sake of clarity, again only the results for **TPCb** in dichloromethane were chosen, providing four quasi-reversible oxidation waves, with the onset of the first oxidation (E_{ox}) at 0.37 eV and the onset of the first reduction (E_{red}) at −1.43 eV. The IP and EA energy levels were thus estimated to be −5.17 eV and −3.37 eV, respectively ($E_{HOMO} = -(4.80 + E_{ox})$, $E_{LUMO} = -(4.80 + E_{red})$).[26] Small variations were found for **TPCa** and **TPCc** (Fig. S7, ESI†). The enlarged π-system of **TPC** is thus fully reflected in the narrower energy gap compared to the reported c-**HBC** (Scheme 1).[13,27] Moreover, the higher HOMO levels of **TPC**s indicate that they are stronger donors than c-**HBC**.

Since the steric congestion around the periphery leads to non-planarity of **TPC**s, we deal with different conformational isomers, which not only were predicted from DFT calculations, but also evidenced by NMR analysis. Fig. 3 displays two distinct DFT calculated structures of **TPCa**. These calculations revealed that **TPCs** adopt at least more than two distinct conformations with different energies. The frontier molecular orbital profiles indicated that in each conformer the HOMO was one of the radialene π-set and the lowest-energy, spin-allowed excitations were primarily from the HOMO to the LUMO.[13] All of the isomers have more significant deviations from planarity due to enhanced steric interactions, among which two isomers with a butterfly conformation could be identified with lower energies (conf 1 ΔE = 4.34 eV and conf 2 ΔE = 7.33 kcal) than the up-down conformation of four peripheral pyrenes (Fig. 3). Using two dimensional NMR experiments, the proton resonances of **TPCb** could be assigned to their corresponding nuclei. The conformations of the structure of the **TCPb** with the three 2D measurements (^{1}H,^{1}H-COSY; ^{1}H,^{1}H-NOESY and the ^{1}H,^{13}C-HSQC) at 373 K in $C_2D_2Cl_4$ are shown in Fig. S8–S10 (ESI†). Interestingly, the analysis revealed that in all cases the proton resonances appear as two sets of signals with very large splitting, which suggest a different chemical environment for one kind of proton resulting from the significantly twisted geometries in agreement with the butterfly conformations. Due to the magnetic anisotropy of the benzene rings in the highly twisted form, some protons located at similar positions experience different ring current effects. This explains the big difference in chemical shifts of 1 ppm in **TPCc** (positions a1 and a2) given in Fig. S11d (ESI†). NMR measurements

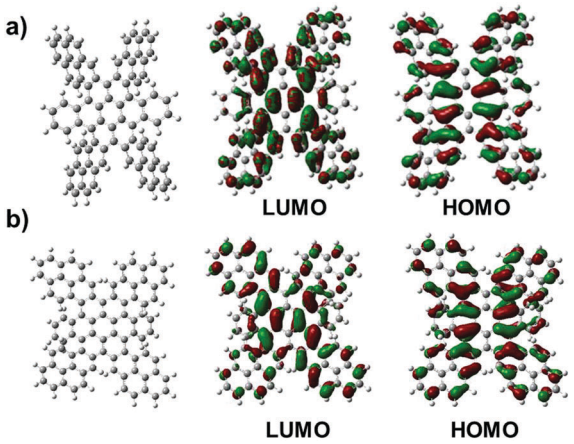

Fig. 3 Optimized structures for **TPCa** and the corresponding frontier molecular orbitals with (a) an up-down conformation and (b) the lowest energy butterfly conformation with two sets of diagonally oriented pyrenes.

at room temperature reveal a broadening of the aromatic signals, due to the hindered conformational stiffness of the molecules, *e.g.* in **TCPb**. In particular, the protons at positions (for numbering please see the picture in Fig. S8, ESI†) i, i′ and b, b′, and c, c′ are in close contact with each other, and the strong dipole–dipole interaction between the protons shortens the T2 time (spin–spin relaxation) similar to a broadening of the peaks. Variant temperature NMR measurements up to 413 K sharpen the signals because of the higher mobility inside the molecules, which average out the strong dipole interactions. Even at 413 K the system has 18 signals instead of the expected 9 signals (two reflection planes and two C_2 symmetry axes) (Fig. S11, ESI†). This can be explained only when each two of the condensed pyrene subunits are inequivalent as in both butterfly conformations.

We further investigated the assembly behavior of **TPCa–c** in bulk films which were prepared by drop-casting a 1,2-dichlorobenzene solution (2 mg mL^{-1}) on a hexamethyldisilazane modified SiO_2 substrate and studied by grazing incidence wide-angle X-ray scattering (GIWAXS in Fig. 4). The patterns reveal significant differences in surface arrangement and order among the three molecules. **TPCa** is oriented face-on towards the surface so that the plane of the aromatic core is almost parallel to the substrate as evident from the distinct out-of-plane reflection in the wide-angle range corresponding to a π-stacking distance of 0.35 nm (Fig. 4a). The scattering intensity shows a certain broad maximum in the off-meridional (marked in red in Fig. 4a), which might originate from the distortion of the core. Interestingly, a further pronounced reflection emerges on the same out-of-plane pattern which corresponds to a *d*-spacing of 1.05 nm, which might be attributed to a helical packing of **TPCa**. In this packing model, the molecules are rotated by *ca.* 60° towards each other to result in the same positional order of every 4th molecule within the stack. Due to the face-on arrangement, these stacks "stand" on the surface and form a hexagonal array with a unit cell parameter of 1.75 nm as derived from the positions of the in-plane reflections. The attachment of *tert*-butyl groups significantly changes the surface arrangement of **TPCb** into an edge-on fashion (Fig. 4b). The π-stacking reflection is located in-plane, while the peak

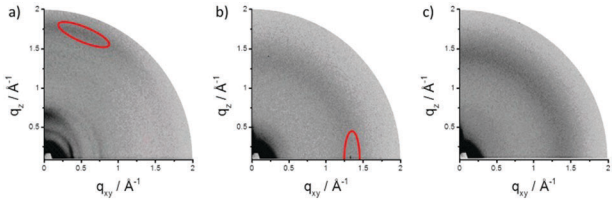

Fig. 4 GIWAXS patterns for thin films of (a) **TPCa**, (b) **TPCb** and (c) **TPCc**. Reflections corresponding to molecular stacking are indicated in red.

related to the stacks can be found on the out-of-plane pattern. Due to the bulkiness of the *tert*-butyl substituents which lower the molecular interactions, the stacking distance increases to 0.45 nm. As an additional effect of the steric influence, the order decreases as evidenced by the small number and low intensity of the reflections. The introduction of flexible dodecyloxy side chains in **TPCc** leads to even an amorphous organization so that the corresponding pattern does not exhibit any reflection.

In summary, a series of tetrapyrene-fused coronenes was designed and synthesized. The combination of regio-controlled functionalization of 2,7-substituted pyrenes and the solution-mediated Scholl reaction was demonstrated as a feasible and efficient approach towards these structure-defined PAHs. These supersized PAHs are of synthetic and photo-physical interest because of their unusual shape with contorted, double coves and zig-zag edges proven by NMR. Our study revealed that these molecules are stronger donor materials compared to conventional discotic coronenes or hexabenzocoronenes, and with a high tendency towards aggregation in both solution and a solid film. Moreover, these discotic molecules can be employed as the building block to construct even more expanded graphene segments which would shine light on the structure–property relations of nanographenes.

This work was financially supported by the Graphene Flagship (CNECT-ICT-604391) and the Gutenberg Research College of the Johannes-Gutenberg University, Mainz. L. Chen is grateful for the financial support from the National Natural Science Foundation of China (51522303, 21602154) and the National Key Research and Development Program of China (2017YFA0207500). Open Access funding provided by the Max Planck Society.

Notes and references

1 A. H. Castro Neto, F. Guinea, N. M. R. Peres, K. S. Novoselov and A. K. Geim, *Rev. Mod. Phys.*, 2009, **81**, 109.
2 C. O. Girit, J. C. Meyer, R. Erni, M. D. Rossell, C. Kisielowski, L. Yang, C. H. Park, M. F. Crommie, M. L. Cohen, S. G. Louie and A. Zettl, *Science*, 2009, **323**, 1705.
3 T. Enoki, S. Fujii and K. Takai, *Carbon*, 2012, **50**, 3141.
4 D. E. Jiang, B. G. Sumpter and S. Dai, *J. Chem. Phys.*, 2007, **126**, 134701.
5 J. S. Wu, W. Pisula and K. Müllen, *Chem. Rev.*, 2007, **107**, 718.
6 A. Narita, X. Feng, Y. Hernandez, S. A. Jensen, M. Bonn, I. A. Verzhbitskiy, C. Casiraghi, M. R. Hansen, A. H. R. Koch, G. Fytas, O. Ivasenko, B. Li, K. S. Mali, T. Balandina, S. Mahesh, S. De Feyter and K. Müllen, *Nat. Chem.*, 2014, **6**, 126.
7 F. Chen and N. J. Tao, *Acc. Chem. Res.*, 2009, **42**, 429.
8 (*a*) L. Chen, Y. Hemandez, X. L. Feng and K. Müllen, *Angew. Chem., Int. Ed.*, 2012, **51**, 7640; (*b*) M. Ball, Y. Zhong, Y. Wu, C. Schenck, F. Ng, M. Steigerwald, S. Xiao and C. Nuckolls, *Acc. Chem. Res.*, 2015, **48**, 267.
9 Z. W. Shi, R. Yang, L. C. Zhang, Y. Wang, D. H. Liu, D. X. Shi, E. G. Wang and G. Y. Zhang, *Adv. Mater.*, 2011, **23**, 3061.
10 F. Shintaro and E. Toshiaki, *Acc. Chem. Res.*, 2013, **46**, 2202.
11 Q. Zhang, H. Q. Peng, G. S. Zhang, Q. Q. Lu, J. Chang, Y. Y. Dong, X. Y. Shi and J. F. Wei, *J. Am. Chem. Soc.*, 2014, **136**, 5057.
12 X. Y. Wang, F. D. Zhuang, R. B. Wang, X. C. Wang, X. Y. Cao, J. Y. Wang and J. Pei, *J. Am. Chem. Soc.*, 2014, **136**, 3764.
13 A. C. Whalley, K. N. Plunkett, A. A. Gorodetsky, C. L. Schenck, C.-Y. Chiu, M. L. Steigerwald and C. Nuckolls, *Chem. Sci.*, 2011, **2**, 132.
14 (*a*) C.-Y. Chiu, B. Kim, A. A. Gorodetsky, W. Sattler, S. Wei, A. Sattler, M. Steigerwald and C. Nuckolls, *Chem. Sci.*, 2011, **2**, 1480; (*b*) S. Xiao, M. Myers, Q. Miao, S. Sanaur, K. Pang, M. Steigerwald and C. Nuckolls, *Angew. Chem., Int. Ed.*, 2005, **44**, 7390; (*c*) K. N. Plunkett, K. Godula, C. Nuckolls, N. Tremblay, A. C. Whalley and S. Xiao, *Org. Lett.*, 2009, **11**, 2225.
15 B. He, A. B. Pun, L. M. Klivansky, A. M. McGough, Y. Ye, J. Zhu, J. Guo, S. J. Teat and Y. Liu, *Chem. Mater.*, 2014, **26**, 3920.
16 L. Chen, S. R. Puniredd, Y.-Z. Tan, M. Baumgarten, U. Zschieschang, V. Enkelmann, W. Pisula, X. Feng, H. Klauk and K. Müllen, *J. Am. Chem. Soc.*, 2012, **134**, 17869.
17 X. Li, Y. Zhu, J. Shao, B. Wang, S. Zhang, Y. Shao, X. Jin, X. Yao, R. Fang and X. Shao, *Angew. Chem., Int. Ed.*, 2012, **51**, 7640.
18 C.-M. Chou, S. Saito and S. Yamaguchi, *Org. Lett.*, 2014, **16**, 2868.
19 C. R. Swartz, S. R. Parkin, J. E. Bullock, J. E. Anthony, A. C. Mayer and G. G. Malliaras, *Org. Lett.*, 2005, **7**, 3163.
20 A. G. Crawford, Z. Liu, I. A. I. Mkhalid, M.-H. Thibault, N. Schwarz, G. Alcaraz, A. Steffen, J. C. Collings, A. S. Batsanov, J. A. K. Howard and T. B. Marder, *Chem. – Eur. J.*, 2012, **18**, 5022.
21 M. Grzybowski, K. Skonieczny, H. Butenschön and D. T. Gryko, *Angew. Chem., Int. Ed.*, 2013, **52**, 9900.
22 S. Tokito, H. Tanaka, K. Noda, A. Okada and Y. Taga, *Appl. Phys. Lett.*, 1997, **70**, 1929.
23 M. Melucci, L. Favaretto, C. Bettini, M. Gazzano, N. Camaioni, P. Maccagnani, P. Ostoja, M. Monari and G. Barbarella, *Chem. – Eur. J.*, 2007, **13**, 10046.
24 R. Abbel, R. van derWeegen, W. Pisula, M. Surin, P. Leclère, R. Lazzaroni, E. W. Meijer and A. P. H. J. Schenning, *Chem. – Eur. J.*, 2009, **15**, 9737.
25 S. Xiao, S. J. Kang, Y. Wu, S. Ahn, J. B. Kim, Y.-L. Loo, T. Siegrist, M. L. Steigerwald, H. Li and C. Nuckolls, *Chem. Sci.*, 2013, **4**, 2018.
26 Y. Zagranyarski, L. Chen, Y. Zhao, H. Wonneberger, C. Li and K. Müllen, *Org. Lett.*, 2012, **14**, 5444.
27 N. J. Tremblay, A. A. Gorodetsky, M. P. Cox, T. Schiros, B. Kim, R. Steiner, Z. Bullard, A. Sattler, W.-Y. So, Y. Itoh, M. F. Toney, H. Ogasawara, A. P. Ramirez, I. Kymissis, M. L. Steigerwald and C. Nuckolls, *ChemPhysChem*, 2010, **11**, 799.